



Exploration and optimization for methylene blue dye removal with modified macadamia nut shell

Yadong Jiang^a, Jianfeng Ye^{b,*}, Qian Feng^a, Wen Yang^a

^aCollege of Environment, Hohai University, Nanjing Jiangsu 210098, P.R. China, Tel. +86 25 83787935; email: jyd@hhu.edu.cn (Y. Jiang), Tel. +86 25 83781619; email: xiaofq@hhu.edu.cn (Q. Feng), Tel. +86 25 83781619; email: 904714138@qq.com (W. Yang)

^bShanghai Academy of Environmental Sciences, No. 508, Qinzhou Road, Shanghai 200233, P.R. China, Tel. +86 21 64085119; Fax: +86 21 64085119; email: yejf99@aliyun.com

Received 11 March 2016; Accepted 9 June 2016

ABSTRACT

A low cost biosorbent, prepared from macadamia nut shell by ultrasonic and alkali treatments, was studied to investigate the mechanism of methylene blue removal and optimization of the adsorption process. The adsorption mechanism was explored through a comparative research with four kinds of adsorbents. Response surface methodology was used to find out the major factors influencing methylene blue adsorption capacity and the interactions between these factors, and optimize the operating variables as well. The results indicated that the modification process changed the surface charge and exposed functional groups on the adsorbent surface. Electrostatic adsorption and hydrogen-bond interaction in the aqueous solution were the major adsorption mechanism. Response surface methodology was applied to develop a second-order polynomial regression model that showed a high coefficient of determination value ($R^2 = 0.9789$) about adsorption process. The optimum conditions were acquired when 220 mg/L solution was contacted with 0.4 g/L adsorbent at initial pH 11 and 120 min, and 444.732 mg/g adsorption capacity was achieved.

Keywords: Macadamia nut shell; Adsorption mechanism; Methylene blue; Optimization; Response surface methodology (RSM)

1. Introduction

The wastewater effluents from industries such as textile, paper, leather, plastics, printing and so on, contain several kinds of synthetic dyestuffs [1,2]. It is estimated that more than 35,000–70,000 million tons of dyes are discharged into the water environment annually [3]. The dyes are characterized by high organic pollutant content, deep colour, and significant serious impact on the water quality, which are released into the environment, causing a high potential risk to human health and ecosystem [4–6]. Methylene blue is the most commonly used substance of dyeing cotton, silk and wood. It can be harmful if it is swallowed, breathed and in contact with the skin. Besides, it can

cause nausea, vomiting, profuse sweating, mental confusion, methemoglobinemia, and even permanent burns to the eyes of human and animals [7,8]. Therefore, an increased interest has been focused on removing of such dyes from the wastewater.

The removal methods of dyes from industrial effluents have been widely studied in recent years such as advanced oxidation processes, chemical precipitation, biological treatment, flocculation, super filter film and adsorption [4,9–12]. Among the numerous techniques for dye removal, adsorption is believed to give the best results as it can be used to remove different types of dyestuffs economically [13]. Activated carbon is the common adsorbent and found to be effective, but high price and hard regeneration limit the wide application [14,15]. Thus, there is a demand for other low-cost, efficient and practical adsorbents for the dye removal.

* Corresponding author.

In recent years, there is growing interest in the production of agricultural and forestry wastes as bio-sorbents because of their abundant resources and cheap prices. Macadamia nut shell is a novel agricultural residue with good chemical stability and steady mechanical strength, which has been used in the removal of heavy metals and dyestuffs successfully in previous studies [16,17]. However, to the best of our knowledge, there have not been any studies in the literature that used chemical-physical modification with Macadamia nut shell as adsorbents. Hence, studies on Macadamia nut shell modification for dyestuffs removal are still insufficient.

Therefore, modified Macadamia nut shell by ultrasonic and alkali treatments as a cheap, excellent and promising adsorbent was tested for enhanced adsorption of methylene blue from aqueous solution. Investigation of the adsorption mechanism and optimization of the adsorption process were the main objectives in this study. The adsorption mechanism was deduced with surface characteristic and pH value, which were characterized by scanning electron microscope (SEM), electron dispersive spectroscopy (EDS), and Fourier transform infrared spectroscopy (FTIR) and thermogravimetric analysis. Response surface methodology (RSM) with central composite design was used for the optimization of methylene blue adsorption by using MMNS. The optimal conditions for adsorption capacity were obtained *via* experimental data by Plackett-Burman and RSM.

2. Materials and methods

2.1. Reagents

Sodium hydroxide (NaOH) and methylene blue ($C_{16}H_{18}ClN_3S$, molecular weight of 319.86 g/mol) were purchased from KeLong Chemical Co. Ltd. (China); hydrochloric acid was purchased from Dongfang Chemical Co. Ltd. (China). All chemical reagents were of analytical grade and all solutions used in the experiments were prepared with distilled water. Pristine macadamia nut shell was obtained from market Nanjing, China.

2.2. Modified macadamia nut shell

2.2.1. Pretreatment

Firstly, pristine macadamia nut shell was immersed into the distilled water at 30°C for 14 d to get rid of the pulp, fly ash and other inorganic impurities. Then, it was dried (at 60°C), crushed and sieved to produce particles of 120 mesh. Finally, the powdered macadamia nut shell (abbreviated as MNS hereinafter) was stored in a desiccator for modification or used for analysis as well as adsorption experiments.

2.2.2. Modified treatment

Firstly, 4 g MNS and 60 mL distilled water were added into 100 mL beaker by ultrasound at 60 w for 120 min. Subsequently, 0.24 g NaOH was added into the beaker, the whole reaction mixture was stirred in a magnetic stirrer at 70°C for 120 min. Finally, the mixtures were washed for several times to the eluent pH neutral and then dried at 60°C to get the modified macadamia nut shell (MMNS). In addition,

4 g MNS and 60 mL distilled water were added into 100 mL beaker by ultrasound at 60 w for 120 min and then dried at 60°C to get the ultrasound-macadamia nut shell (UMNS). 4 g MNS and 0.1 M 60 mL NaOH were added into 100 mL beaker with the magnetic stirrer at 70°C for 120 min and dried at 60°C to get the alkali-macadamia nut shell (AMNS). UMNS and AMNS were used for the analysis in subsequent experimental.

2.3. Absorption experiment

50 mL dye solution with concentration of 200 mg/L and 0.025 g adsorbent were added into the 100 mL Erlenmeyer flasks. The initial pH was adjusted by using 0.1 M (or 1 M) HCl and 0.1 M NaOH. The effect of initial pH on the removal of methylene blue was performed in the range of 2–12. The mixture was shaken at a constant temperature by using the thermostatic shaker at 180 rpm 30°C for 180 min. After achieving sorption equilibrium, the final pH was detected for each solution. The solution that interacted with adsorbent was filtered through a 0.45 mm filter. The concentration of methylene blue in the filtrate was analyzed with the UV-VIS spectrometer at the maximum wavelength of 664 nm [18]. The MMNS after absorbing methylene blue (abbreviated as MB-MMNS hereinafter) was collected for further analysis. All experiments were performed with three replicates and the mean values were used for analysis [4,19].

2.4. Plackett–Burman experiment design

The effect of seven factors including the initial pH, contact time, temperature, initial concentration, dosage, particle size and shaking speed were selected as independent factors and the absorption capacity was chosen to be response to the experiment. The Minitab16 software was applied for experimental design to obtain the significant influence on adsorption. All the parameters including the initial pH, contact time, temperature, initial concentration, adsorbent dosage, particle size and shaking speed varied from the minimum value to the maximum which covered four levels in all. The Minitab16 software required 12 runs for adsorption of methylene blue [20].

2.5. RSM Experimental design

The RSM is a collection of statistical and mathematical techniques based on the fit of a polynomial equation to the experimental data [21]. Which is applied to evaluate the effect of factors and their interaction on the system response. And then, it can be used to determine the best condition for the adsorption process and the effects of different parameters on adsorption behaviour [17,22,23].

RSM mainly contains three steps: design of adsorption experiments, response surface modelling and optimization of best conditions [22]. Based on the results of Plackett-Burman, four parameters including the initial pH, contact time, dosage and initial concentration were selected as the independent variables for the experimental design. Eq. (1) could be used to transform the real value (X_i) into the coded value (x_i) in the determinate experimental design [24,25]:

$$x_i = \frac{X_i - X_i^*}{\Delta X_i} \quad (1)$$

where ΔX_i is the distance between the real value in the central point and the real value in the superior or inferior level, X_i^* is the real value in the central point. x_i means the independent variables in coded level, while X_i represents the real value of variables.

A total of 30 runs were performed, including 6 central points, 16 factorial points and 8 axial points. The response variable (absorption capacity) was fitted to a second-order polynomial regression model, expressed by Eq. (2)

$$Y = \beta_0 + \sum_{i=1}^k \beta_i x_i + \sum_{i=1}^k \beta_{ii} x_i^2 + \sum_{i=1}^k \sum_{j=1}^k \beta_{ij} x_i x_j + \varepsilon \quad (2)$$

where Y is the response variable, x_i and x_j are the coded variables, β_0 , β_i , β_{ii} and β_{ij} are the regression coefficients (β_0 is the constant term, β_i is the linear coefficient, β_{ii} is the quadratic coefficient, and β_{ij} is the interaction coefficient), ε is the model error [24].

The analysis of variance (ANOVA) was used to test the significance of the independent variables and their interactions. Results and the statistical significance of the quadratic model were assessed with t-ratio, p-value, F-value, degrees of freedom (df), correlation coefficient (R^2), adjusted correlation coefficient (R^2_{adj}), sum of squares (SS), mean sum of squares (MSS), and chi-square (χ^2) [26]. The Design Expert 8.0.6 software (Stat-Ease, Inc., Minneapolis, USA) was applied for elaboration of the adsorption experimental design, evaluation of the model and optimization of the best conditions. And the Matlab R2010a software (MathWorks, Inc., Natick, USA) was used to draw the graphs. The experiment design was listed in Table S1.

2.6. Analytic methods

The pH measurement was conducted by using the hand-held pH meter (HACH, America) [19]. The concentration of the residual dye was measured by using the UV-VIS spectrometer (ALPHA-1506, China). The specific surface area, total pore volume and average pore diameter of adsorbents were calculated by the automatic specific surface area/pore size distribution measurement (BelSorp Max, Japan). The surface functional groups and structure of adsorbents were conducted with the FTIR (Nexus870, USA) [11,27]. The surface features of adsorbents were performed by the SEM (HITACHI-S-4800N, Japan) [28]. The element compositions of adsorbents were investigated using the EDS (EX-250, Japan). The thermal stabilities of adsorbents were determined using the thermogravimetric analysis (TGA) (Pyris 1 DSC, USA) [4].

3. Results and discussion

3.1. Characterization and investigation of mechanism

3.1.1. SEM analysis and aperture size

Morphological microstructures of MNS, UMNS, AMNS, MMNS and MB-MMNS were observed by the Scanning electron micrograph (Fig. S1). There into Fig. S1(a, b, c, g, h) were the profile of adsorbents, and the Fig. S1(d, e, f, j, k) were the surface of adsorbents. The MNS surface appears planar, without any porous structure, just with some cracks on

it (Fig. S1(d)). The lamellar curly profile of adsorbents was clearly observed in Fig. S1(a, b, c, g).

The UMNS, AMNS and MMNS external surface appeared to have lots of cavities and increasing surface roughness on account of the corrosion and zerteilung after the ultrasonic or alkali modification (Fig. S1(e, g, j)) [29]. However, the surface of MB-MMNS became smooth like a milk biscuit (Fig. S1(k)) and profile void space was filled with methylene blue (Fig. S1(h)), and because of that, the adsorption occurred after the contact of MMNS with methylene blue solution. As shown in Fig. S2, the particle size distribution of adsorbents was almost the same, but the mean particle size of the UMNS, AMNS and MMNS were bigger than that of MNS since the rinsing process drained a part of small size adsorbents.

The values of specific surface area, total pore volume and average pore diameter of adsorbents were listed in Table S2. The BET surface area of the MMNS was found to be 0.0305 m²/g, with total pore volume of 0.0026 cm³/g, and average pore diameter 345.38 nm. The data also confirmed that MMNS was predominantly macroporous. Compared with MNS, the specific surface area of MMNS was smaller, and the average pore diameter was higher. Hence, combining with the data of UMNS and AMNS, the specific surface area and the average pore diameter could increase due to the ultrasonic and alkali processes, respectively.

3.1.2. EDS and FTIR analysis

The EDS corresponding element compositions listed in Table S3 indicated that the adsorbents mainly consisted of oxygen and carbon, and trace amounts of sodium which came from the alkali modification. The large proportions of oxygen and carbon attributed to the cellulose and lignin in adsorbents. After the alkali modification, the contents of oxygen had a slightly increase, and the carbon decreased slightly, resulting from the modification with alkali removed fats, waxes, lignin and hemicelluloses from the adsorbents surfaces thus revealing hydroxyl groups [29]. As can be seen from Fig. S1(i, l), the distributions of oxygen, carbon and sodium (existing in the structure of MMNS) were almost uniform. The number of dots with carbon was clearly larger and more intense than those of carbon and sodium, which was consistent with the contents of oxygen, carbon and sodium.

The FTIR spectra of MNS, UMNS, AMNS, MMNS and MB-MMNS in Fig. 1, demonstrated some major differences between the five samples clearly. As can be observed from the curve of MNS, the pronounced peak located at 3,402.6 cm⁻¹ might be assigned to the O–H stretching vibration of hydroxyl groups [30,31]. A band at 2,902.4 cm⁻¹ was assigned to the C–H stretching vibrations of methyl and methylene groups, in consistent with the result of J.S. Cao [4]. The band at 1,738.8 cm⁻¹ could be attributed to C=O stretching vibrations in alkenes groups and carboxyl [32]. The bands in the region 1,609.5 cm⁻¹ to 1,465.2 cm⁻¹ were assigned to C=C stretching, which could be attributed to the presence of aromatic or benzene rings in lignin [33,34]. The band at 1,033 cm⁻¹ might be attributed to C–O stretching in carboxyl acids, alcohols and phenols [35]. What is more, the curve of UMNS was similar to MNS. Hence, chemical bonds and functional groups remained the same basically after the ultrasonic modification. By contrast, despite the curve

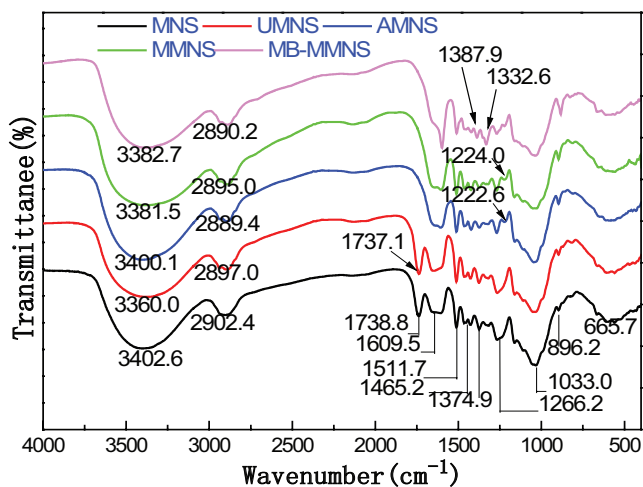


Fig. 1. FTIR spectra of MNS, UMNS, AMNS, MMNS and MB-MMNS.

of AMNS and MMNS were also similar to that of MNS, the peak located at $1,738.8\text{ cm}^{-1}$ (MNS) and $1,737.1\text{ cm}^{-1}$ (UMNS) vanished eventually. The results gained above indicated that the functional groups of MNS had been converted to ionization after the modification with NaOH [8]. In addition, new peaks with C–O bend stretching vibration appeared at $1,222.6\text{ cm}^{-1}$ (AMNS) and $1,224.0\text{ cm}^{-1}$ (MMNS), respectively, after the alkali modification due to that more hydroxyl units were presented resulting from the disruption of cellulose and lignin structures [36]. Fig. 1 also gave the FTIR spectra of MB-MMNS. The new band generated at $1,387.9\text{ cm}^{-1}$ and $1,332.6\text{ cm}^{-1}$ could be ascribed to C=N and C–N bend stretching vibrations, respectively. And the changes in FTIR spectra confirmed the adsorption of methylene blue on MMNS.

3.1.3. TGA analysis

The thermogravimetric weight loss curves of MNS, UMNS, AMNS and MMNS are depicted in Fig. 2. The thermal stability of adsorbents under air atmosphere from 20°C to 700°C with an increase rate of $20^\circ\text{C}/\text{min}$ was evaluated. As to the adsorbents, there were three main weight-loss steps. Initially, there was a slight decline in the mass of MNS, UMNS, AMNS and MMNS with 11.88%, 5.27%, 6.82% and 7.60% up to 100°C , respectively, as the temperature went up to 100°C , due to the release of moisture from adsorbents [37]. The amplitude of substance mass reduction of UMNS, AMNS and MMNS was lesser than that of MNS, probably because of the low humidity of adsorbents caused by the ultrasound and alkali modification. Afterwards, the main degradation step presenting weight loss was recorded within the temperature of 260°C – 400°C , which could be ascribed to the cellulose degradation, including depolymerisation and decomposition of the saccharide rings [38,39], and the breakage of the functional groups and side chains in the lignin, such as –OH, –COOH and C–C bonds [40]. The final step mainly took place above the temperature 400°C . The weight loss attributed to the ring-opening reaction as well as the formation of the cross-linked and condensed aromatic structures in lignin at high temperature [41]. As shown in Fig. 2, the pyrolysis temperature of the AMNS and MMNS

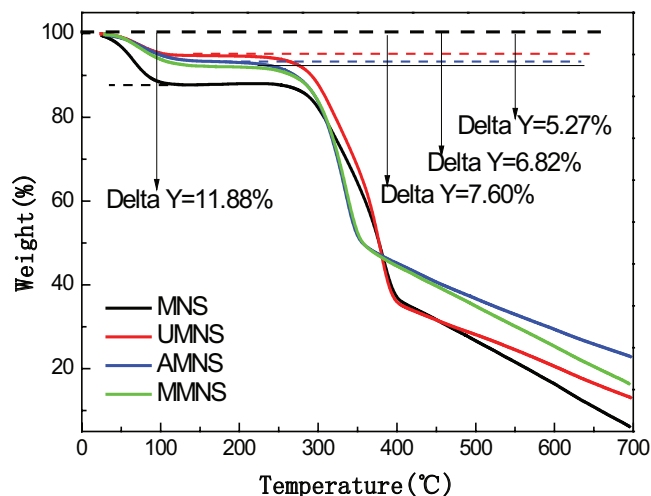


Fig. 2. TGA analysis diagram of MNS, UMNS, AMNS and MMNS.

went down than that of MNS and UMNS due to the alkali modification. However, the prepared and applied adsorbents well proved to be much appropriate for the real field application of MWNS in air atmosphere.

3.1.4. Influence of pH

pH of the solution has been recognized as one of the most important factors influencing any adsorption process [6,8]. It impacts not only the degree of ionization, the adsorbent surface charge and the dissociation of functional groups on the adsorbent, but also the chemical properties of the dye solution [42]. The effect of initial pH on the adsorption of methylene blue by using adsorbents was shown in Fig. 3. As observed, it can be seen that the adsorption of methylene blue was strongly pH-dependent. The adsorption capacity increased from 12.14 mg/g to 174.91 mg/g , 17.89 mg/g to 201.75 mg/g , 23.22 mg/g to 365.97 mg/g and 33.72 mg/g to 377.41 mg/g , respectively, as the pH increased from 2.09 to 11.54 by applying MNS, UMNS, AMNS and MMNS as the adsorbents, in consistent with the result of Shamik Chowdhury and Khalifaoui Amela [42,43]. At low initial pH value, protonation of the functional groups on the adsorbents surface took place easily in the solution while methylene blue, a basic dye, would be positively charged [44], which decreased the adsorption capacity because of electrostatic repulsion [43]. As the initial pH increased, a proportional increase in adsorption took place due to the successive deprotonation of positively charged functional groups and electrostatic attraction between adsorbents and methylene blue [44,42]. The Fig. 3 revealed that the adsorption capacities of AMNS and MMNS were higher than those of MNS and UMNS, which could be attributed to zeta potential changes in the surface electric charge of AMNS and MMNS (Fig. 4). From these zeta potential curves, it can be seen that the pH_{PZC} was around 4.02, 4.10, 7.80 and 8.01 for MNS, UMNS, AMNS and MMNS, respectively. When $\text{pH} > \text{pH}_{\text{PZC}}$ it was observed that adsorbents exhibited negative surface charge, which could facilitates the electrostatic attraction of the methylene blue ions [45,46]. Moreover, a similar behaviour was observed for the methylene blue dye adsorption on diatomite [47].

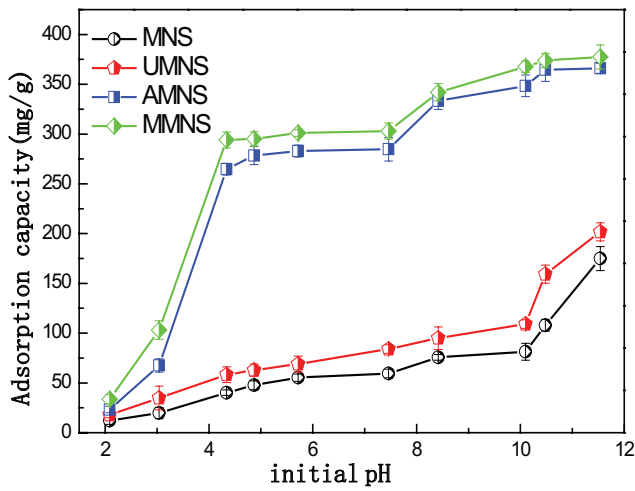


Fig. 3. The effects of pH on methylene blue by MNS, UMNS, AMNS and MMNS (conditions: temperature 30°C; adsorbent dosage 0.5 g/L; stirring rate 180 rpm; react time 180 min; initial concentration 200 mg/L).

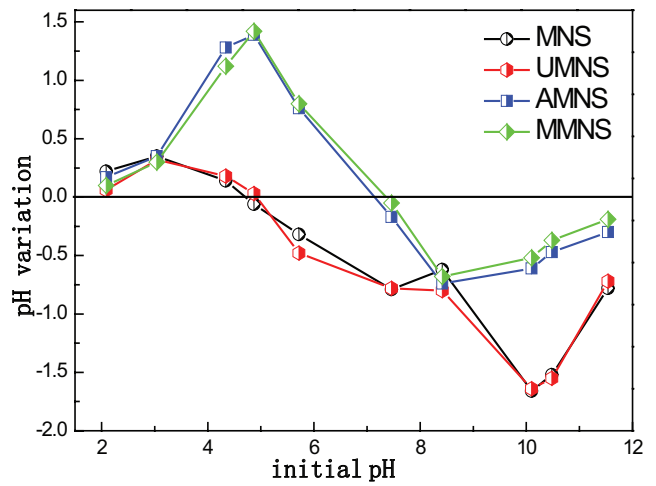


Fig. 5. pH variation curves of MNS, UMNS, AMNS and MMNS.

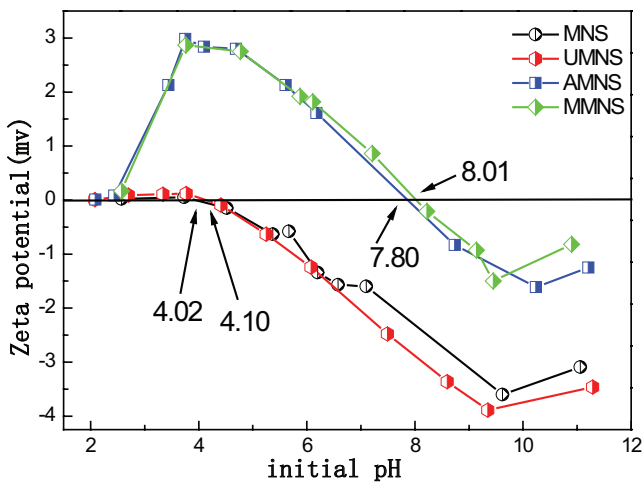


Fig. 4. Zeta-potential curves of MNS, UMNS, AMNS and MMNS.

Fig. 5 showed the variation of pH (expressed in Eq. (3)) with the increasing initial pH for the four kinds of adsorbents (MNS, UMNS, AMNS and MMNS). pH variation (pH_v) increased first and then decreased as the initial pH increased.

$$pH_v = \text{initial pH} - \text{final pH} \quad (3)$$

Through analysis discovery, initial pH_v increased due to that the functional groups on the surface of adsorbents became protonated in the high-acid solution which was caused by the declining final pH. Afterwards, the adsorption capacity increased as the initial pH increased. And partial hydrogen ions were replaced by methylene blue ions. Then, the hydrogen ions diffused into the solution and reacted with hydroxyl ions to reach the acid-base neutralization which could lead to the decrease of pH gradually.

3.1.5. Adsorption mechanism

Combined with the analysis of characterization, the ultrasonic and alkali modification of MMNS exhibited higher adsorption capacities on methylene blue ions than MNS. The adsorption capacity could be improved not only by ultrasonic modification due to the increased specific surface area, but also by alkali modification because of the lignocellulosic materials which could cause swelling, resulting in an increase in the degree of polymerization, a decrease in crystallinity, separation of structural linkages between lignin and carbohydrates and disruption of the lignin structure [29,36]. However, the adsorption capacity of alkali treatment turned out to be better than that of ultrasonic treatment, which resulted from the fact that the alkali treatment was the major factor impacting the modified process.

Electrostatic adsorption and hydrogen bonding mechanisms could account for the uptake of methylene blue by the adsorbents as suggested in Fig. 6. In this connection, it must be pointed out that methylene blue is a cationic dye containing amine groups within its structure. In the solution, methylene blue can be dissociated into MB^+ and Cl^- ions. The negative surface charge of adsorbents and the methylene blue ions had an electrostatic adsorption in the solution. In addition, adsorption of methylene blue on the surface of adsorbents may be attributed to the formation of surface hydrogen bonds between the hydroxyl groups and the nitrogen atoms of methylene blue.

3.2. Analysis of RSM

The Plackett–Burman experiment design was applied to evaluate the significance effects of the seven factors mentioned above on adsorption of methylene blue. It could be seen from the Table S1, initial pH, contact time, initial concentration and dosage were selected to be the parameter variables in the research for RSM by their p-values (<0.05 , significant at 5% level), respectively. Simultaneously, the polynomial equation in coded form was determined and evaluated to demonstrate the adsorption capacity by using Design-Expert 8.0.6 software, as shown in Eq. (4). Among

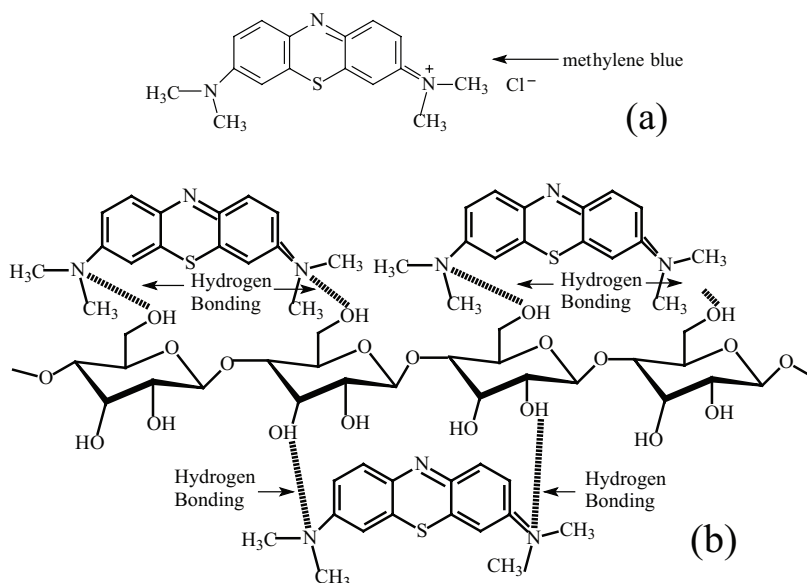


Fig. 6. (a) Chemical structures of methylene blue and (b) the adsorption mechanisms of methylene blue on MMNS.

runs, 1–6 at the centre point were used to determine the experimental error [48].

$$\begin{aligned}
 Y = & 368.73 + 20.54x_p - 26.12x_t - 2.04x_d + 19.57x_c - 14.26x_p x_t \\
 & + 0.13x_p x_d + 10.19x_p x_c + 4.28x_t x_d + 3.83x_t x_c + 1.12x_d x_c \\
 & - 0.34x_p^2 - 15.17x_t^2 + 1.95x_d^2 - 2.35x_c^2
 \end{aligned} \quad (4)$$

where Y is the adsorption capacity of MMNS (mg/g), x_p is coded values of initial pH, x_t is coded values of contact time, x_d is coded values of MMNS dosage and x_c is coded values of initial concentration.

Eq. (4) provided a good visualization of the effects of each parameter, their interaction and quadratic on the response. On one hand, the negative values in the equation indicated that these terms decreased the response. On the other hand, the positive values increased the response [49,50]. Parameters of the experiments and the comparison between actual and predicted values for the adsorption capacity were demonstrated in Table S4.

The statistical significance of the model for adsorption was evaluated by the ANOVA and the obtained results of the sum of squares, DF, mean square, F-values and p-values which were presented in Table S5. The Model F-value of 49.81 implied that the model was significant [48]. That values of "Prob > F" were less than 0.01% confirmed that the model terms were significant. In this case, initial pH (x_p), contact time (x_t), initial concentration (x_c), interaction terms ($x_p x_t$, $x_p x_d$, $x_p x_c$) and quadratic term (x_t^2) were significant model terms, whereas other terms were insignificant to the response [20]. The "Lack of Fit F-value" of 6.74 expressed that the Lack of Fit was significant. The chance of the occurrence of large "Lack of Fit F-value" because of noise is only 2.41% [51].

The comparison of the actual and predicted adsorption capacities confirmed that the determination coefficients (R^2) and the adjusted R^2 (R^2_{adj}) values for the quality of the models aggrandized. Higher value of R^2 was closer to unity as

it would provide the predicted value closer to the actual value for adsorption capacity in the response [51,52]. In this research, the R^2 value for Eq. (4) was 0.9789, which indicated that most of the data variability in the response was explained by the statistical model. The high correlation between the predicted and the actual values were shown in Fig. S3(A). The R^2_{adj} corrected the R^2 value for the number of terms and the sample size in the model. The values of R^2_{adj} was 0.9593, which was found to be close to R^2 [26]. The accuracy and reliability of the experiments conducted were indicated by the low coefficient of variation (C.V.%) of 2.33% [53]. The "Pred R-Squared" of 0.8850 was in reasonable agreement with the "Adj R-Squared", which also confirmed the significance of the model. "Adeq Precision" measured the signal to noise ratio. And a ratio greater than 4 was desirable. In this study, the ratio of 32.164 indicated an adequate signal. This model could be used to navigate the design space. The normal probability of the residuals was shown in Fig. S3(B). The normal probability plot of the residuals was an important diagnostic tool to detect and explain the systematic departures from the assumption that errors were normally distributed and independent with each other, and that the error variance was homogeneous [54]. The normal probability of residuals implied no serious violation of the assumptions underlying the analyses nearly. Meanwhile, it also confirmed the independence of the residuals and normality assumptions [26].

The statistical tests demonstrated that the second-order polynomial regression model presented a good correlation between the predicted and the actual values. It could be applied to simulate the adsorption process and predict the adsorption capacity with different combinations in the design range.

The statistically significant second-order polynomial regression equations of the model were represented through the three dimensional (3D) response surface plots to understand the interaction of the parametric variations and the optimal design condition of the adsorption process.

The influence of the four different parametric variables (initial pH, contact time, dosage and initial concentration) on the response was visualized in the 3D response surface plots (Fig. S4(a)–(f)).

Fig. S4(a) showed the 3D response surface plot of the combined effect of initial pH and the contact time on methylene blue adsorption capacity with other parameter constants ($x_d = 0$ and $x_c = 0$). Fig. S4(a) showed that adsorption capacity increased with either the increase of initial pH ranging from 10 to 11 or the decrease of contact time ranging from 180 to 120 min. The maximum adsorption capacity (414.146 mg/g) could be obtained under this condition (the initial pH 11, contact time 120 min, adsorbent dosage 0.5 g/L and initial dye concentration 200 mg/L). It was obvious that higher initial pH could improve the adsorption capacity because the surface of adsorbent might be negative charged due to the increasing electrostatic interactions between cation dye molecules, which was also observed in Fig. S4(b) and Fig. S4(c).

Fig. S4(c) showed the 3D response surface plot of the combined effects of the initial pH and the initial concentration on methylene blue adsorption capacity with other parameter constants ($x_p = 0$ and $x_d = 0$). The dye adsorption capacity increased with the increase in initial pH ranging from 10 to 11 as well as the initial concentration ranging from 180 to 220 mg/L. Under the optimal condition (initial pH = 11, initial concentration 220 mg/L, adsorbent dosage 0.5 g/L and contact time 150 min), the maximum adsorption capacity (416.324 mg/g) could be obtained. The increase of the initial dye concentration was conducive to the adsorption process during which the adsorbent surface groups contacted with dye molecules better, thus the adsorption capacity increased, which was also observed in Fig. S4(e) and (f).

Fig. S4(f) showed the 3D response surface plot of the combined effects of the dosage and the initial concentration on methylene blue adsorption capacity with other parameter constants ($x_p = 0$ and $x_i = 0$). The dye adsorption capacity increased with the decrease of the adsorbent dosage ranging from 0.6 to 0.4 g/L or with the increase of the initial concentration ranging from 180 to 220 mg/L. The maximum adsorption capacity (388.806 mg/g) could be obtained under the optimal condition (adsorbent dosage 0.4 g/L, initial concentration 220 mg/L, contact time 150 min and initial pH 10). It was quite obvious that the adsorption capacity of methylene blue increased when the adsorbent dosage decreased gradually due to a high percentage of adsorption with adsorbent at a low dosage level, which was also observed in Fig. S4(b) and (d).

The second-order polynomial regression model on the basis of RSM suggested the optimal condition of different independent variables in range. According to the Design Expert 8.0.6 software, the optimal condition was obtained when 220 mg/L methylene blue solution was contacted with 0.4 g/L MNS at initial pH 11 and contact time 120 min, to achieve the maximum theoretical adsorption (444.732 mg/g) of methylene blue. The experimental adsorption value of the methylene blue under the same optimal condition was obtained as 444.214 ± 0.911 mg/g (mean \pm SD of three replicates), which was very close to the optimized value by model.

4. Conclusion

In this research, the modified MMNS was proved to be an effective adsorbent to remove methylene blue from aqueous solutions. For the surface characterization and mechanism studies, the SEM, EDS, FTIR, XPS and TGA indicated that the surface of MMNS became bumpy, and appeared more hydroxy groups on the adsorbent surface by modification process. In addition, the mechanism of adsorption involved ion exchange and hydrogen bonding in aqueous solutions. In the RSM studies, the initial pH, contact time, initial concentration and dosage were main factors influencing on adsorption. Through the experiments and model simulation, a second-order polynomial regression was obtained. According to the model, the optimal condition was as follows: initial pH 11, contact time 120 min, adsorbent dosage 0.4 g/L and initial concentration 220 mg/L. And the experimental as well as theoretical adsorption capacities were 444.214 mg/g and 444.732 mg/g, respectively.

Acknowledgements

This work was supported by the Key Special Program for the Pollution Control (2012ZX07101-003 and 2011ZX07301-002), the Natural Science Foundation of Shanghai (Grant Number: 16ZR1429800), the Shanghai Committee of Science and Technology (Grant Number: 14DZ1208200).

References

- [1] M. ud Din, H.N. Bhatti, M. Yasir, A. Ashraf, Direct dye biosorption by immobilized barley husk, *Desal. Water Treat.*, 57 (2016) 9263–9271.
- [2] M. Asif Tahir, H.N. Bhatti, M. Iqbal, Solar Red and Brittle Blue direct dyes adsorption onto Eucalyptus angophoroides bark: equilibrium, kinetics and thermodynamic studies, *J. Environ. Chem. Eng.*, 4 (2016) 2431–2439.
- [3] S. Liu, Y. Ding, P. Li, K. Diao, X. Tan, F. Lei, Y. Zhan, et al., Adsorption of the anionic dye Congo red from aqueous solution onto natural zeolites modified with N,N-dimethyl dehydroabietylamine oxide, *Chem. Eng. J.*, 248 (2014) 135–144.
- [4] J.S. Cao, J.X. Lin, F. Fang, M.T. Zhang, Z.R. Hu, A new adsorbent by modifying walnut shell for the removal of anionic dye: Kinetic and thermodynamic studies, *Bioresour. Technol.*, 163 (2014) 199–205.
- [5] H.N. Bhatti, S. Nausheen, Equilibrium and kinetic modeling for the removal of Turquoise Blue PG dye from aqueous solution by a low-cost agro waste, *Desal. Water Treat.*, 55 (2015) 1943–1944.
- [6] H.N. Bhatti, S. Noreen, N. Tahir, S. Ilyas, U.H. Siddiqua, Equilibrium, thermodynamic and kinetic studies for biosorption of Terasil Brown 2RFL from contaminated water using economical biomaterial, *Mediterranean J. Chem.*, 4 (2015) 239–251.
- [7] M.Z. Kabir, A.K. Mukarram, S.B. Mohamad, Z. Alias, S. Tayyab, Characterization of the binding of an anticancer drug, lapatinib to human serum albumin, *J. Photochem. Photobiol. B*, 160 (2016) 229–239.
- [8] A. Mittal, R. Ahmad, I. Hasan, Biosorption of Pb^{2+} , Ni^{2+} and Cu^{2+} ions from aqueous solutions by L-cystein-modified montmorillonite-immobilized alginate nanocomposite, *Desal. Water Treat.*, (2015) 1–18.
- [9] J. Mittal, A. Mittal, Green chemistry for dyes removal from wastewater: research trends and applications, 409 (2015).
- [10] M. Naushad, A. Mittal, M. Rathore, V. Gupta, Ion-exchange kinetic studies for Cd(II), Co(II), Cu(II), and Pb(II) metal ions over a composite cation exchanger, *Desal. Water Treat.*, 54 (2015) 2882–2890.

- [11] A. Mittal, R. Ahmad, I. Hasan, Iron oxide-impregnated dextrin nanocomposite: synthesis and its application for the biosorption of Cr(VI) ions from aqueous solution, *Desal. Water Treat.*, 57 (2016) 15133–15145.
- [12] A. Mittal, L. Kurup, Column operations for the removal and recovery of a hazardous dye 'acid red - 27' from aqueous solutions, using waste materials – bottom ash and de-oiled soya, *Ecol. Environ. Conser.*, 13 (2006) 181–186.
- [13] G.Z. Kyzas, N.K. Lazaridis, A.C. Mitropoulos, Removal of dyes from aqueous solutions with untreated coffee residues as potential low-cost adsorbents: equilibrium, reuse and thermodynamic approach, *Chem. Engin. J.*, 189 (2012) 148–159.
- [14] R. Zhang, J. Zhang, X. Zhang, C. Dou, R. Han, Adsorption of Congo red from aqueous solutions using cationic surfactant modified wheat straw in batch mode: kinetic and equilibrium study, *J. Taiwan Inst. Chem. Eng.*, 45 (2014) 2578–2583.
- [15] C. Xia, Y. Jing, Y. Jia, D. Yue, J. Ma, X. Yin, Adsorption properties of congo red from aqueous solution on modified hectorite: kinetic and thermodynamic studies, *Desalination*, 265 (2011) 81–87.
- [16] G.E.J. Poinern, G. Senanayake, N. Shah, X.N. Thi-Le, G.M. Parkinson, D Fawcett, Adsorption of the aurocyanide, $Au(CN)_2^-$ complex on granular activated carbons derived from macadamia nut shells-A preliminary study, *Minerals Engineering*, 24 (2011) 1694–1702.
- [17] O.P. Junior, A.L. Cazetta, R.C. Gomes, É.O. Barizão, I.P.A.F. Souza, A.C. Martins, T. Asefa, V.C. Almeida, Synthesis of ZnCl₂-activated carbon from macadamia nut endocarp (*Macadamia integrifolia*) by microwave-assisted pyrolysis: optimization using RSM and methylene blue adsorption, *J. Anal. Appl. Pyrolysis*, 105 (2014) 166–176.
- [18] A.M.M. Vargas, A.L. Cazetta, M.H. Kunita, T.L. Silva, V.C. Almeida, Adsorption of methylene blue on activated carbon produced from flamboyant pods (*Delonix regia*): study of adsorption isotherms and kinetic models, *Chem. Eng. J.*, 68 (2011) 722–730.
- [19] S.M. Miller, J.B. Zimmerman, Novel, bio-based, photoactive arsenic sorbent: TiO₂-impregnated chitosan bead, *Water Res.*, 19 (2010) 5722–5729.
- [20] M.Ş. Tanyildizi, Modeling of adsorption isotherms and kinetics of reactive dye from aqueous solution by peanut hull, *Chem. Eng. J.*, 168 (2011) 1234–1240.
- [21] M.A. Bezerra, R.E. Santelli, E.P. Oliveira, L.S. Villar, L.A. Escalera, Response surface methodology (RSM) as a tool for optimization in analytical chemistry, *Talanta*, 76 (2008) 965–977.
- [22] T. Shojaeimehr, F. Rahimpour, M.A. Khadivi, M. Sadeghi, A modeling study by response surface methodology (RSM) and artificial neural network (ANN) on Cu²⁺ adsorption optimization using light expanded clay aggregate (LECA), *J. Ind. Eng. Chem.*, 20 (2014) 870–880.
- [23] Y. Jin, Y. Wu, J. Cao, Y. Wu, Optimizing decolorization of Methylene Blue and Methyl Orange dye by pulsed discharged plasma in water using response surface methodology, *J. Taiwan Inst. Chem. Eng.*, 45 (2014) 589–595.
- [24] A.R. Amani-Ghadim, S. Aber, A. Olad, H. Ashassi-Sorkhabi, Optimization of electrocoagulation process for removal of an azo dye using response surface methodology and investigation on the occurrence of destructive side reactions, *Chemical Engineering and Processing: Process Intensification*, 64 (2013) 68–78.
- [25] E.K. Baghkheirati, M.B. Bagherieh-Najjar, Modelling and optimization of Ag-nanoparticle biosynthesis mediated by walnut green husk extract using response surface methodology, *Mater. Lett.*, 171 (2016) 166–170.
- [26] K.P. Singh, S. Gupta, A.K. Singh, S. Sinha, Optimizing adsorption of crystal violet dye from water by magnetic nanocomposite using response surface modeling approach, *J. Hazard. Mater.*, 186 (2011) 1462–1473.
- [27] D. Hritcu, D. Humelnicu, G. Dodi, M.I. Popa, Magnetic chitosan composite particles: evaluation of thorium and uranyl ion adsorption from aqueous solutions, *Carbohydr. Polym.*, 87 (2012) 1185–1191.
- [28] G. Sharma, M. Naushad, D. Pathania, A. Mittal, G.E. El-desoky, Modification of Hibiscus cannabinus fiber by graft copolymerization: application for dye removal, *Desal. Water Treat.*, 54 (2015) 3114–3121.
- [29] S. Chakraborty, S. Chowdhury, P.D. Saha, Adsorption of Crystal Violet from aqueous solution onto NaOH-modified rice husk, *Carbohydr. Polym.*, 86 (2011) 1533–1541.
- [30] A.C. Martins, O. Pezoti, A.L. Cazetta, K.C. Bedin, D.A.S. Yamazaki, G.F.G. Bandoch, T. Asefa, et al., Removal of tetracycline by NaOH-activated carbon produced from macadamia nut shells: kinetic and equilibrium studies, *Chem. Engin. J.*, 260 (2015) 291–299.
- [31] A. Mittal, M. Naushad, G. Sharma, Z.A. AlLothman, S.M. Wabaidur, M. Alam, Fabrication of MWCNTs/ThO₂ nanocomposite and its adsorption behavior for the removal of Pb(II) metal from aqueous medium, *Desal. Water Treat.* (2015) 1–7.
- [32] M.K. Dahri, M.R.R. Kooch, L.B.L. Lim, Water remediation using low cost adsorbent walnut shell for removal of malachite green: equilibrium, kinetics, thermodynamic and regeneration studies, *J. Environ. Chem. Engin.*, 2 (2014) 1434–1444.
- [33] T.H. Liou, Development of mesoporous structure and high adsorption capacity of biomass-based activated carbon by phosphoric acid and zinc chloride activation, *Chem. Engin. J.*, 158 (2010) 129–142.
- [34] V.M. Vučurović, R.N. Razmovski, U.D. Miljić, V.S. Puškaš, Removal of cationic and anionic azo dyes from aqueous solutions by adsorption on maize stem tissue, *J. Taiwan Inst. Chem. Eng.*, 45 (2014) 1700–1708.
- [35] R.H. Hesas, A. Arami-Niya, W.M.A.W. Daud, J.N. Sahu, Preparation of granular activated carbon from oil palm shell by microwave-induced chemical activation: optimisation using surface response methodology, *Chem. Eng. Res. Des.*, 91 (2013) 2447–2456.
- [36] W.S. Wan Ngah, M.A.K.M. Hanafiah, Removal of heavy metal ions from wastewater by chemically modified plant wastes as adsorbents: a review, *Bioresour. Technol.*, 99 (2008) 3935–3948.
- [37] V. Nair, A. Panigrahy, R. Vinu, Development of novel chitosan-lignin composites for adsorption of dyes and metal ions from wastewater, *Chem. Eng. J.*, 254 (2014) 491–502.
- [38] T. Hosoya, H. Kawamoto, S. Saka, Cellulose-hemicellulose and cellulose-lignin interactions in wood pyrolysis at gasification temperature, *J. Anal. Appl. Pyrolysis*, 80 (2007) 118–125.
- [39] J. Lédé, Cellulose pyrolysis kinetics: an historical review on the existence and role of intermediate active cellulose, *J. Anal. Appl. Pyrolysis*, 94 (2012) 17–32.
- [40] M. Zhang, F.L.P. Resende, A. Moutsoglou, D.E. Raynie, Pyrolysis of lignin extracted from prairie cordgrass, aspen, and Kraft lignin by Py-GC/MS and TGA/FTIR, *J. Anal. Appl. Pyrolysis*, 98 (2012) 65–71.
- [41] Z. Luo, S. Wang, X. Guo, Selective pyrolysis of Organosolv lignin over zeolites with product analysis by TG-FTIR, *J. Anal. Appl. Pyrolysis*, 95 (2012) 112–117.
- [42] S. Chowdhury, R. Mishra, P. Saha, P. Kushwaha, Adsorption thermodynamics, kinetics and isosteric heat of adsorption of malachite green onto chemically modified rice husk, *Desalination*, 265 (2011) 159–168.
- [43] K. Amela, M.A. Hassena, D. Kerroum, Isotherm and kinetics study of biosorption of cationic dye onto banana peel, *Energy Procedia*, 19 (2012) 286–295.
- [44] H. Fan, L. Zhou, X. Jiang, Q. Huang, W. Lang, Adsorption of Cu²⁺ and methylene blue on dodecyl sulfobetaine surfactant-modified montmorillonite, *Appl. Clay Sci.*, 95 (2014) 150–158.
- [45] S. Chen, Q. Yue, B. Gao, X. Xu, Equilibrium and kinetic adsorption study of the adsorptive removal of Cr(VI) using modified wheat residue, *J. Colloid. Interf. Sci.*, 349 (2010) 256–264.
- [46] K. Pillay, E.M. Cukrowska, N.J. Coville, Multi-walled carbon nanotubes as adsorbents for the removal of parts per billion levels of hexavalent chromium from aqueous solution, *J. Hazard. Mater.*, 166 (2009) 1067–1075.
- [47] J. Zhang, Q. Ping, M. Niu, H. Shi, N. Li, Kinetics and equilibrium studies from the methylene blue adsorption on diatomite treated with sodium hydroxide, *Appl. Clay Sci.*, 83 (2013) 12–16.

- [48] J.N. Sahu, J. Acharya, B.C. Meikap, Optimization of production conditions for activated carbons from tamarind wood by zinc chloride using response surface methodology, *Bioresour. Technol.*, 101 (2010) 1974–1982.
- [49] A.M.M. Vargas, A.C. Martins, V.C. Almeida, Ternary adsorption of acid dyes onto activated carbon from flamboyant pods (*Delonix regia*): analysis by derivative spectrophotometry and response surface methodology, *Chem. Eng. J.*, 195 (2012) 173–179.
- [50] W. Jiang, A.J. Joens, D.D. Dionysios, K.E. O’Shea, Optimization of photocatalytic performance of TiO₂ coated glass microspheres using response surface methodology and the application for degradation of dimethyl phthalate, *J. Photochem. Photobiol. A*, 262 (2013) 7–13.
- [51] M.A. Ahmad, R. Alrozi, Optimization of preparation conditions for mangosteen peel-based activated carbons for the removal of Remazol Brilliant Blue R using response surface methodology, *Chem. Eng. J.*, 165 (2010) 883–890.
- [52] S. Chatterjee, A. Kumar, S. Basu, S. Dutta, Application of response surface methodology for methylene blue dye removal from aqueous solution using low cost adsorbent, *Chem. Eng. J.*, 181 (2012) 289–299.
- [53] R. Sen, T. Swaminathan, Response surface modeling and optimization to elucidate and analyze the effects of inoculum age and size on surfactin production, *Biochem. Eng. J.*, 21 (2004) 141–148.
- [54] H.L. Liu, Y.W. Lan, Y.C. Cheng, Optimal production of sulphuric acid by *Thiobacillus thiooxidans* using response surface methodology, *Process Biochem.*, 39 (2004) 1953–1961.

Supporting information

Table S1
Experiment design for RSM

Variable	Unit	Notation	Limits					
			-2	-1	0	1	2	
Initial pH	X_p	—	pH	11.5	11	10.5	10	9.5
Contact time	X_t	min	T	90	120	150	180	210
Dosage	X_d	g/l	D	0.3	0.4	0.5	0.6	0.7
Initial concentration	X_c	mg/l	C_0	160	180	200	220	240

Table S2
The specific surface area, total pore volume and average pore diameter of MNS, UMNS, AMNS and MMNS

Contents	MNS	UMNS	AMNS	MMNS
Specific surface area ($a_{s,BET}$ (m ² /g))	0.1860	0.2444	0.0121	0.0305
Total pore volume (cm ³ /g)	0.0064	0.0067	0.0056	0.0026
Average pore diameter (nm)	138.11	109.22	228.56	345.38

Table S3
Element composition of MNS, UMNS, AMNS and MMNS

Element	MNS		UMNS		AMNS		MMNS	
	Weight percentage (%)	Atomic percentage (%)						
C	79.01	83.37	78.76	82.98	75.33	80.88	71.89	77.72
O	20.99	16.63	21.24	17.02	22.55	17.94	25.94	21.06
Na	—	—	—	—	2.12	1.18	2.17	1.23

Table S4
Experimental design for adsorption capacity of methylene blue

Run	Design matrix								Experimental results	Predicted results
	Real values ^a				Coded values ^b					
	X_p	X_t	X_d	X_c	x_p	x_t	x_d	x_c		
1	10.5	150	0.5	200	0	0	0	0	361.52 ± 2.97	368.73
2	10.5	150	0.5	200	0	0	0	0	371.20 ± 1.09	368.73
3	10.5	150	0.5	200	0	0	0	0	369.01 ± 2.03	368.73
4	10.5	150	0.5	200	0	0	0	0	371.44 ± 2.21	368.73
5	10.5	150	0.5	200	0	0	0	0	371.44 ± 1.24	368.73
6	10.5	150	0.5	200	0	0	0	0	368.10 ± 0.93	368.73
7	10	120	0.6	220	-1	-1	1	1	345.27 ± 1.56	344.36
8	10	120	0.4	220	-1	-1	-1	1	361.74 ± 0.67	355.02
9	10.5	150	0.5	160	0	0	0	-2	318.70 ± 2.87	320.19
10	10	180	0.6	220	-1	1	-1	1	330.92 ± 1.68	330.40
11	11	120	0.4	180	1	-1	1	-1	380.05 ± 2.54	380.50
12	10	120	0.4	180	-1	-1	1	-1	334.98 ± 2.32	331.02
13	10.5	150	0.5	200	0	0	-2	0	373.21 ± 2.89	380.61
14	10	180	0.6	220	-1	1	1	1	331.21 ± 1.73	336.86
15	11	180	0.6	180	1	1	-1	-1	297.30 ± 0.56	298.14
16	11	120	0.4	220	1	-1	-1	1	447.44 ± 3.76	444.74
17	10	180	0.6	180	-1	1	1	-1	305.56 ± 2.43	308.20
18	9.5	150	0.5	200	-2	0	0	0	326.73 ± 1.59	326.29
19	10.5	150	0.5	200	0	0	2	0	375.37 ± 2.01	372.45
20	10.5	210	0.7	200	0	2	0	0	268.63 ± 0.74	255.81
21	11	180	0.6	220	1	1	1	1	364.89 ± 2.32	370.06
22	10.5	150	0.5	240	0	0	0	2	395.43 ± 3.02	398.47
23	10	120	0.4	180	-1	-1	-1	-1	351.38 ± 2.33	346.16
24	10	180	0.4	180	-1	1	-1	-1	300.66 ± 1.34	306.22
25	10.5	90	0.3	200	0	-2	0	0	342.99 ± 1.02	360.29
26	11.5	150	0.5	200	2	0	0	0	403.48 ± 3.03	408.45
27	11	120	0.4	180	1	-1	-1	-1	405.18 ± 3.15	395.12
28	11	180	0.6	220	1	1	-1	1	363.50 ± 2.12	363.08
29	11	180	0.6	180	1	1	1	-1	298.33 ± 1.21	300.64
30	10	120	0.4	220	1	-1	1	1	444.58 ± 2.23	434.60

^a X_p = pH, X_t = contact time (min), X_d = dosage (g), X_c = initial concentration (mg/l).

^b $x_p = (X_p - 10.5) / 0.5$, $x_t = (X_t - 150) / 30$, $x_d = (X_d - 0.5) / 0.1$, $x_c = (X_c - 200) / 20$.

Table S5
Analysis of variance (ANOVA) for response surface quadratic model

Source	Sum of squares	df	Mean squares	F value	P-value Prob > F
Model	48,112.24	14	3,436.59	49.81	<0.0001
x_p	10,129.37	1	10,129.37	146.80	<0.0001
x_t	16,378.65	1	16,378.65	237.37	<0.0001
x_d	99.73	1	99.73	1.45	0.2479
x_c	9,187.49	1	9,187.49	133.15	<0.0001
$x_p x_t$	3,254.82	1	3,254.82	47.17	<0.0001
$x_p x_d$	0.28	1	0.28	0.00	0.9501
$x_p x_4$	1,660.21	1	1,660.21	24.06	0.0002
$x_t x_d$	292.99	1	292.99	4.25	0.0571
$x_t x_c$	234.29	1	234.29	3.40	0.0852
$x_d x_c$	20.19	1	20.19	0.29	0.5965
x_p^2	3.24	1	3.24	0.05	0.8312
x_t^2	6,309.71	1	6,309.71	91.44	<0.0001
x_d^2	104.59	1	104.59	1.52	0.2372
x_c^2	152.01	1	152.01	2.20	0.1584
Residual	1,035.01	15	69.00		
Lack of fit	963.53	10	96.35	6.74	0.0241
Pure error	71.48	5	14.30		
Correlation Total	49,147.25	29			
R-squared	0.9789		Adj R-squared	0.9593	
Pred R-squared	0.8850		Adeq precisor	32.164	
Std. Dev.	8.31		Mean	356.00	
C.V.%	2.33		PRESS	5,652.87	

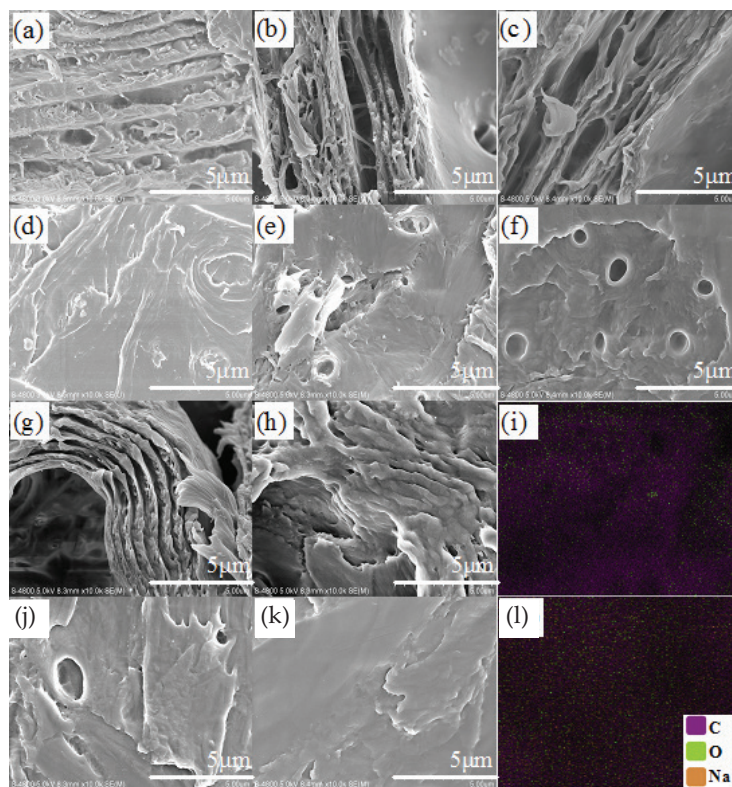


Fig. S1. SEM micrographs of (a, d) MNS; (b, e) UMNS; (c, f) AMNS; (g, j) MMNS; (h, k) MB-MMNS and EDS spectra of (i) MNS and (l) MMNS.

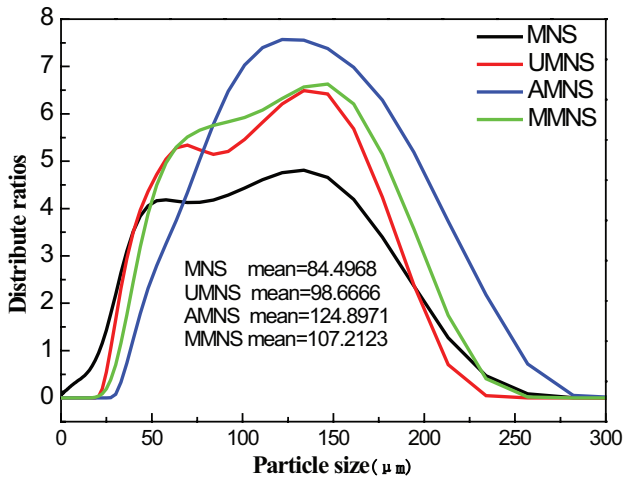


Fig. S2. Particle size distribution of MNS; UMNS; AMNS; MMNS.

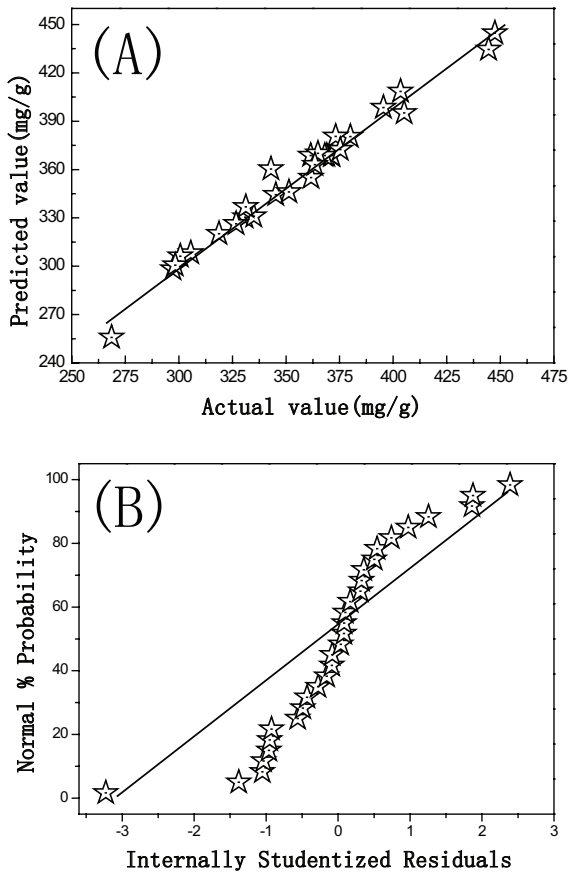


Fig. S3. (A) Correlation of actual and predicted values, (B) the normal probability plot of the internally studentized residuals.

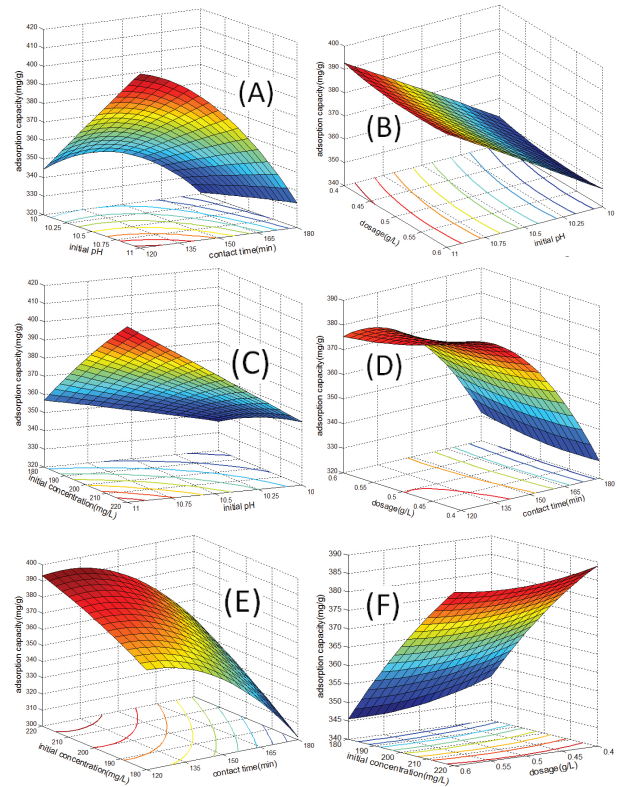


Fig. S4. Three-dimensional plots of model for adsorption capacity: (A) initial pH and contact time; (B) initial pH and dosage; (C) initial pH and initial concentration; (D) dosage and contact time; (E) contact time and initial concentration; (F) dosage and initial concentration on methylene blue adsorption capacity.